7. Egan, R. W., Galen, P. H., Beveridge, G. C., Phillips, G. B. & Marnett, L. J. *Prostaglandins* **16**, 861–869 (1978).
8. Mason, R. T. & Staszewska-Barczak, J. *J. clin. exp. Pharmac. Physiol.* **6**, 678–685 (1979).
9. Takeguchi, C., Kohno, E. & Sih, C. J. *Biochemistry* **10**, 2372–2376 (1971).
10. Winter, C. A., Risley, E. A. & Nuss, G. W. *Proc. Soc. exp. Biol. Med.* **111**, 554–557 (1962).
11. Branceni, D., Azadian-Boulanger, G. & Jequier, R. *Archs int. Pharmacodyn.* **152**, 15–24 (1964).
12. Kemper, F. & Ameln, G. *Z. ges. exp. Med.* **131**, 407–415 (1959).
13. Flückiger, E., Schlach, W. & Taeschler, M. *Schweiz. med. Wschr.* **93**, 1232–1237 (1963).

A model of the nerve impulse using two first-order differential equations

J. L. Hindmarsh & R. M. Rose

Department of Applied Mathematics and Astronomy and Department of Physiology, University College, Cardiff, Cardiff CF1 1XL, UK

The Hodgkin–Huxley model[1] of the nerve impulse consists of four coupled nonlinear differential equations, six functions and seven constants. Because of the complexity of these equations and the necessity for numerical solution, it is difficult to use them in simulations of interactions in small neural networks. Thus, it would be useful to have a second-order differential equation which predicted correctly properties such as the frequency–current relationship. Fitzhugh[2] introduced a second-order model of the nerve impulse, but his equations predict an action potential duration which is similar to the inter-spike interval[3] and they do not give a reasonable frequency–current relationship. To develop a second-order model having few parameters but which does not have these disadvantages, we have generalized the second-order Fitzhugh equations[2], and based the form of the functions in the new equations on voltage-clamp data obtained from a snail neurone. We report here an unexpected property of the resulting equations—the x and y null clines in the phase plane lie close together when the phase point is on the recovery side of the phase plane. The resulting slow movement along the phase path gives a long inter-spike interval, a property not shown clearly by previous models[2,4]. The model also predicts the linearity of the frequency–current relationship, and may be useful for studying detailed interactions in networks containing small numbers of neurones.

Although our model may be seen as a generalization of the Fitzhugh equations[2], it can be developed from first principles if it is assumed that the rate of change of membrane potential depends linearly on z (the current passed through the electrode), and y (an intrinsic current), and depends nonlinearly on membrane potential, giving

$$\dot{x} = -a(f(x) - y - z) \tag{1}$$

We assume also that the rate of change of intrinsic current is given by

$$\dot{y} = b(g(x) - y) \tag{2}$$

In these equations, a and b are constants, and equation (2) has a form which ensures that the time course of z in voltage-clamp conditions is exponential (see equation (4)). This is a simplification which ignores the voltage-dependence of the time constants.

To determine the form of $f(x)$ and $g(x)$ in equations (1) and (2), a large cell from the visceral ganglion of the pond snail, *Lymnaea stagnalis*, was clamped to a range of different voltages (x_p), and the initial ($z_{x_p}(0)$) and steady-state ($z_{x_p}(\infty)$) values of the clamping current were measured, giving a conventional[5] current–voltage plot (Fig. 1). As the cell fires repetitively in the resting state, the membrane potential was biased initially by adjusting z so that the cell just stopped firing. This corresponds to an artificial stable equilibrium point, and will be used as the origin ($x = 0$, $y = 0$) in the phase plane. In the current–voltage plot (Fig. 1), the scale is also positioned so that the current required to maintain the equilibrium voltage is at the origin

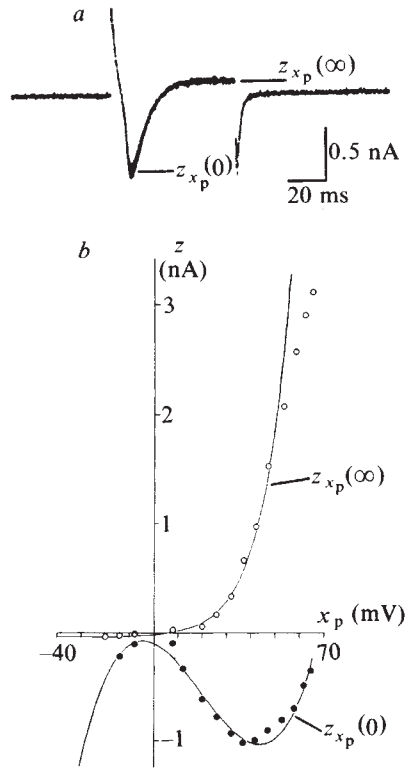

Fig. 1 Voltage-clamp data on which the model is based. In these experiments, the brain of the pond snail *L. stagnalis* was pinned out in a chamber with a sylgard base, and the outer sheath softened using pronase enzyme for a few minutes before recording. The bathing solution had the following composition (mM): Na^+, 24.0; K^+, 2.0; Ca^{2+}, 4.0; Mg^{2+}, 2.0; Cl^-, 38.0; $H_2PO_4^{2-}$, 0.1; Na–HEPES, 35.4. A large cell (~200 μm) in the visceral ganglion was impaled with a bevelled glass microelectrode filled with 3 M KCl, and having a resistance of 4–5 MΩ. The cell was clamped using the single-electrode voltage-clamp technique of Wilson and Goldner[7]. *a*, Current change recorded for a voltage step (x_p) of 25 mV from the equilibrium point (cell held at an actual potential of −60 mV, which is the equilibrium point, $x = 0$, in the measurements). The initial ($z_{x_p}(0)$, or peak inward) and final ($z_{x_p}(\infty)$, or steady-state outward) currents are indicated, the final currents being measured after 60 ms in this case. *b*, Initial and final currents obtained from records such as shown in *a* are plotted for different values of clamp potential (x_p) measured from the equilibrium point. Negative values of z are inward, and positive values are outward currents. Final currents were measured 100 ms after onset of voltage step. Different animal than in *a*, but curves are typical for this cell (experiment repeated five times). The $z_{x_p}(0)$ points have been fitted by the least-squares method, using the cubic equation $f(x) = cx^3 + dx^2 + ex + h$, where $c = 0.00017$, $d = 0.001$, $e = 0.01$ and $h = 0.1$. The $z_{x_p}(\infty)$ points were fitted by an exponential of the form $g(x) = q\,e^{rx} - s$, where $q = 0.024$, $r = 0.088$ and $s = 0.046$.

($z = 0$). Therefore, at the equilibrium position $x = y = \dot{x} = \dot{y} = z = 0$. The time course of the current, after the onset of a step in voltage to x_p, is given (from equation (1) with $\dot{x} = 0$) by

$$z_{x_p}(t) = f(x_p) - y(t) \tag{3}$$

where y satisfies equation (2) with $x = x_p$.

Therefore, $z_{x_p}(t)$ is given by

$$z_{x_p}(t) = f(x_p) - g(x_p)(1 - e^{-bt}) \tag{4}$$

and hence

$$z_{x_p}(0) = f(x_p), \text{ and } z_{x_p}(\infty) = f(x_p) - g(x_p) \tag{5}$$

To obtain $f(x_p)$, the values of the initial currents ($z_{x_p}(0)$; Fig. 1*b*) were fitted by a cubic equation. To obtain $g(x_p)$, an exponential function was fitted to the value of the final currents ($z_{x_p}(\infty)$; Fig. 1*b*), and $g(x_p)$ was obtained from equation (5). The time constant b was estimated from voltage-clamp current records

0028–0836/82/100162—03$01.00

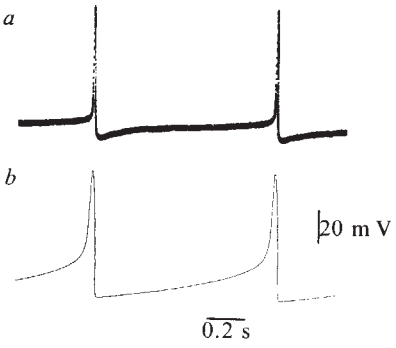

Fig. 2 Comparison between *a*, actual and *b*, calculated waveforms for the same cell as in Fig. 1*b*. The calculated waveform is the solution to equations (7) and (8) for a current of $z = 0.008$, with the constants $a = 5{,}400\ \text{mV s}^{-1}$, nA^{-1}, $b = 30\ \text{s}^{-1}$ and using the functions $f(x)$ and $g(x)$ shown in Fig. 1*b*. Numerical solutions were obtained using the Runge–Kutta–Merson method[8] with variable step length. In these calculations we found that repetitive firing occurred down to $z = -0.026$ rather than $z = 0$ as expected (procedure outlined in the text). This was due to the approximations adopted, which slightly changed the values of $f(x)$ and $g(x)$ at the origin. As the computed equilibrium point is at $z = 0.034$ ($=0.008 \pm 0.026$) in Fig. 4. The recorded action potentials were obtained in current-clamp conditions with an experimental z value of 0.04 and were photographed ~1 min after imposing the current step.

(Fig. 1*a*), which were assumed to follow an exponential time course, and the time constant a was obtained by applying a current step to the system at rest in the equilibrium position (0, 0). If the step in current is $z(t) = z_p$ for $t \geq 0$ then a may be obtained from the slope of the voltage change immediately after the onset of the current-clamp step. This is given by equation (1) with $f(0) = 0$ and $y(0) = 0$:

$$\dot{x}(0) = az_p \tag{6}$$

Thus the assumed form for our equations is

$$\dot{x} = -a(f(x) - y - z) \tag{7}$$

$$\dot{y} = b(f(x) - q\,e^{rx} + s - y) \tag{8}$$

where $f(x) = cx^3 + dx^2 + ex + h$, and a–h, q, r and s are constants.

After measuring a and b, and fitting cubic and exponential functions to the $z_{xp}(0)$ and $z_{xp}(\infty)$ data of Fig. 1*b*, the solutions of equations (7) and (8) were obtained by numerical integration.

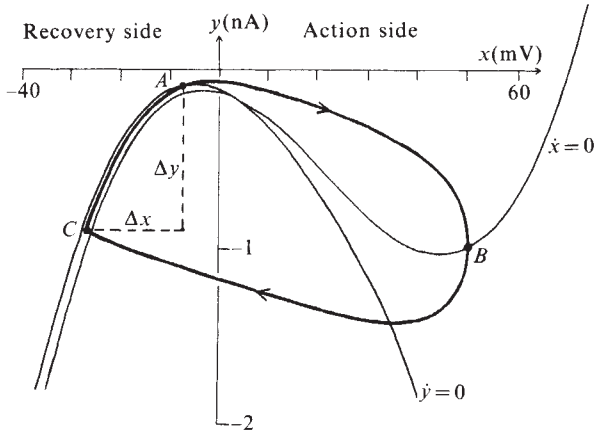

Fig. 3 Phase plane representation of the limit cycle solution to equations (7) and (8). The values of the constants are the same as in Fig. 2, except that a z value of 0.033 has been used so that the equilibrium point can be more clearly distinguished. The $\dot{x} = 0$ curve has been displaced horizontally to the right by 2–3 mV so that the separation between the x and y null clines on the recovery side of the diagram can be seen more easily. The $\dot{x} = 0$ curve is similar to that of Fitzhugh[2], but the $\dot{y} = 0$ curve bends round to follow the $\dot{x} = 0$ curve in the lower left-hand quadrant, which is significantly different from the Fitzhugh model. The limit cycle is divided into an action potential phase ($A \rightarrow B \rightarrow C$) and a recovery phase ($C \rightarrow A$), during which the phase point moves slowly between the x and y null clines. The differences Δx and Δy are, respectively, the changes in membrane potential and intrinsic current during recovery.

Figure 2 compares the calculated $x(t)$ waveform with that recorded from the cell. The model clearly predicts a ratio of spike duration to inter-spike interval which is similar to that actually recorded, although the calculated action potential is of rather longer duration than the recorded spike; the pacemaker potential also rises to a higher threshold in the model. Some of these differences may be corrected by taking into account the voltage dependency of the time constants, but these modifications are not introduced here because they detract from the simplicity of the model.

Although this model is not as accurate as more complicated models of repetitive firing[6], it has a conceptual advantage which becomes apparent when the oscillation is plotted onto the phase plane. The main difference between this model and that of Fitzhugh[2] is the introduction of $g(x)$ into the equation for $\dot{y}$. By using the phase diagram (Fig. 3) it becomes easy to understand why this modification is so important in lengthening the recovery phase between successive action potentials. In the phase plane, when the limit cycle crosses the $\dot{x} = 0$ curve at C (Fig. 3), it is constrained to move along the narrow path between the $\dot{x} = 0$ and $\dot{y} = 0$ curves. Because the phase path is so close to both the x and y null clines, progress along the limit cycle will be much slower from C to A (the pacemaker or recovery phase) than from A through B to C (the action potential part of the cycle). By contrast, in Fitzhugh's model the $\dot{x} = 0$ and $\dot{y} = 0$ curves diverge markedly on both sides of the diagram, so that x and y change almost as rapidly during the pacemaker phase as during the spike itself.

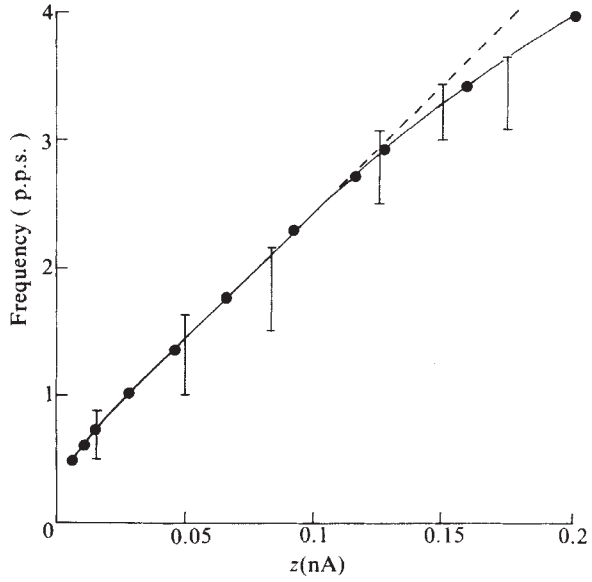

Fig. 4 Comparison of the calculated and experimental frequency–current relationship (pulses per second). The calculated frequencies (●) were derived from numerical integration of equations (7) and (8) using the same parameter values as in Fig. 2 but with different values of z. Calculated frequencies are plotted relative to the computed equilibrium point ($z = -0.026$; see Fig. 2). Experimental z values were measured relative to the experimental equilibrium point (at which $z = 0$; there were no action potentials). Over most of the range there is a linear relationship between frequency and applied current, with both experimental and calculated curves having a similar slope. At higher values of z, the calculated curve and the experimental points begin to approach a limiting frequency at a similar z value, although the experimental points appear to fall off more sharply from linearity (broken line) than the theoretical prediction. This particular cell also shows adaptation of firing frequency to an applied current step, so that the values for the experimental frequencies lie within the upper (=initial frequency in response to step) and lower (=final frequency) limits of the bar lines. Thus a precise comparison cannot be made because the model has not yet been modified to include adaptation. Experimental points were obtained from a different animal than that used in Fig. 1*b*, but the experiment was repeated four times and gave consistent results.

Numerical solution may also be used to predict the frequency–current relationship. The computed values of the frequency are linearly related to the current (Fig. 4) and compare reasonably well with the experimental values. It is also possible to derive an expression for the frequency–current relationship fairly simply. From equations (1) and (2) we see that

$$b\dot{x} + a\dot{y} = ab(g(x) - f(x)) + abz \quad (9)$$

Then the expression $g(x) - f(x)$ $(= -z(\infty)$; equation (5)) may be approximated for $x < 0$ by a small positive constant M (see $z_x(\infty)$ in Fig. 1*b*). Integrating (9) we obtain

$$b\Delta x + a\Delta y = abMT + abzT \quad (10)$$

where Δx and Δy are the changes in the values of x and y during recovery (from C to A in Fig. 3), which occurs in time T, say. If we ignore the spike duration, the frequency f of oscillation is given by

$$f = \frac{1}{T} = \frac{ab(z + M)}{b\Delta x + a\Delta y} \quad (11)$$

from which we can see that, to the extent that Δx and Δy are independent of z, f is linearly related to z (see Fig. 4).

The model therefore predicts the frequency–current relationship as well as giving a reasonably accurate representation of the time course of the membrane potential change. It also provides a simple explanation of why the recovery time is much longer than the spike duration. Because these equations are simpler to understand than the four-dimensional Hodgkin–Huxley equations[1], and can be solved numerically in a shorter time, they may be useful in studying small neural networks.

We thank Dr W. A. Wilson for supplying us with further information on the single electrode voltage-clamp, and Mr W. L. Barry and Mr T. Ford for constructing the voltage-clamp apparatus.

Received 1 September 1981; accepted 26 January 1982.

1. Hodgkin, A. L. & Huxley, A. F. *J. Physiol., Lond.* **117,** 500–554 (1952).
2. Fitzhugh, R. *Biophys. J.* **1,** 445–466 (1961).
3. Jack, J. J. B., Noble, D. & Tsien, R. W. (eds) *Electric Current Flow in Excitable Cells*, 330 (Clarendon, Oxford, 1975).
4. Kokoz, Yu. M. & Krinskii, V. J. *Biofizika* **18,** 878–885 (1973).
5. Frank, K. & Tauc, L. in *Cellular Function of Membrane Transport* (ed. Hoffman, J.) 113–134 (Prentice-Hall, New Jersey, 1964).
6. Connor, J. A. & Stevens, C. F. *J. Physiol., Lond.* **213,** 31–53 (1971).
7. Wilson, W. A. & Goldner, M. M. *J. Neurobiol.* **6,** 411–422 (1975).
8. Merson, R. H. in *Proc. of Symp. on Data Processing* (Weapons Research Establishment, South Australia, 1957).

Induction of helical liposomes by Ca^{2+}-mediated intermembrane binding

Ke-Chun Lin*, Robert M. Weis & Harden M. McConnell

Stauffer Laboratory for Physical Chemistry, Stanford University, Stanford, California 94305, USA

Extensive freeze-fracture electron microscopic studies of Ca^{2+}-containing mixtures of an acidic phospholipid (cardiolipin) and phosphatidylcholines[1–5], have revealed certain replica features which have been interpreted as regions of membrane–membrane attachment[3–5]. Spin-label paramagnetic resonance spectra of mixtures of another acidic phospholipid (phosphatidylserine) and phosphatidylcholines have provided evidence for Ca^{2+}-mediated lateral phase separations of the acidic phospholipids[6–8], and their involvement in intermembrane binding[7]. We report here that in the presence of Ca^{2+}, binary mixtures of cardiolipin and phosphatidylcholines readily form tightly folded single- and double-helical liposomes; we invoke membrane–membrane attachment to explain this phenomenon.

* Permanent address: Department of Biophysics, Beijing Medical College, Beijing, China.

Ethanolic solutions of bovine heart cardiolipin (Ca^{2+}-free; Sigma) and dimyristoylphosphatidylcholine (Sigma) were evaporated to dryness to form binary mixtures containing 37 mol % cardiolipin (1.7 mg total lipid). The lipid was dissolved in chloroform/methanol (10:1 v/v) and evaporated to dryness, then 160 μl phosphate-buffered saline (PBS) were added with or without 2 mM EDTA and the mixture was incubated at 45 °C for 5 min, vortexed for 10–15 s, then diluted 20-fold with PBS. All experiments were carried out at 25–26 °C, well above the chain-melting transition of dimyristoylphosphatidylcholine (23 °C).

We used two experimental protocols: (1) after addition of PBS + EDTA and vortexing, the dilution with PBS contained no Ca^{2+}. The sample was placed on a microscope slide with an elevated coverslip (100 μm) and a concentrated $CaCl_2$ solution (0.01–1 M) was added from one side. Ca^{2+} ions gradually diffused through the solution, allowing observation of helix formation (see Fig. 1*a–d*). (2) For the mixture incubated without EDTA, the subsequent dilution with PBS contained various low concentrations of Ca^{2+} (10^{-6}–10^{-3} M).

Single and double helix formation, observed using protocol (1), is shown in Fig. 1. Long tubes were often observed in the absence of Ca^{2+}, together with liposomes having typical irregular shapes. The presence of regular tubes and irregular liposomes may be explained by possible lipid compound formation and phase separations in binary mixtures of these lipids[9]. The tubes were almost perfect cylinders, although end defects were frequently seen, and were usually multilamellar but occasionally unilamellar, as judged by microscopic observation of pronounced brownian motion, characteristic of unilamellar liposomes[10]. Photobleaching recovery experiments measuring diffusion parallel to the long axis of the tubes yielded lateral diffusion coefficients typical of fluorescent lipid probes ($D \sim 10^{-8}$ cm^2 s^{-1}).

Protocol (1) provided evidence that the rate of helix formation increased with increasing Ca^{2+} concentration. Protocol (2) permitted the determination of the minimum concentration of Ca^{2+} ion required for helix formation; compared with controls (no Ca^{2+}), significantly more helices were formed at Ca^{2+} concentrations as low as 10^{-6} M.

The thermodynamic driving force for helix formation is the Ca^{2+}-mediated membrane–membrane binding. At higher Ca^{2+} concentrations, helices rapidly collapse on themselves forming a variety of more complex structures. It is possible that helices represent kinetic intermediates in the Ca^{2+}-mediated transformation of tubes to more complex structures, as each step of helix formation represents an increase in the area of membrane–membrane contact. The formation of a typical single helix is simple; it is initiated at one end, and is smooth and continuous. However, double-helix formation is sometimes complex; it initiates from a hairpin loop and progresses in a stepwise manner. A complete regular double helix with no loose ends can initiate at a hairpin loop but not in the centre of a tube; this requires sliding as well as twisting of one tube relative to the other (see Fig. 1*a–c*).

The rate at which helices form in the presence of Ca^{2+} is consistent with earlier proposals concerning Ca^{2+}-mediated lateral phase separations of acidic phospholipids[6–8], and with the rates of lateral diffusion of these lipid molecules reported here. Ca^{2+} chelation by phosphate groups should be favoured when these groups have a three-dimensional configuration, rather than a two-dimensional configuration provided by a single membrane.

The forces opposing helix formation are weak. The shear modulus of a fluid membrane is essentially zero; a negligible force is required to twist one region of a lipid tube relative to another. We observed no distortion of the circularity of the tubes, thus there was no detectable volume or surface area change of the tubes on helix formation. Note that the outer diameter of the double helix in Fig. 1 is twice the diameter of the tube. No stretch or compression elastic energy is required to convert a cylindrical tube into a helix because lipids on the

0028–0836/82/100164—02$01.00